Chinese Chemical Letters 35 (2024) 110283

Contents lists available at ScienceDirect

Chinese Chemical Letters

journal homepage: www.elsevier.com/locate/cclet

A matrix metalloproteinase-sensitive hydrogel combined with photothermal therapy for transdermal delivery of deferoxamine to accelerate diabetic pressure ulcer healing

Haijun Shen[1,*], Yi Qiao[1], Chun Zhang, Yane Ma, Jialing Chen, Yingying Cao, Wenna Zheng

Department of Preventive Medicine and Public Health Laboratory Science, School of Medicine, Jiangsu University, Zhenjiang 212013, China

ARTICLE INFO

Article history:
Received 13 May 2024
Revised 15 July 2024
Accepted 17 July 2024
Available online 18 July 2024

Keywords:
Diabetic pressure ulcer
Transdermal drug delivery
Matrix metalloproteinase-sensitive hydrogel
Antibacterial
Angiogenesis

ABSTRACT

Diabetic pressure ulcers (DPU) are non-healing due to vascular dysfunction and bacterial infection. Early intervention can delay ulcer progression, such as preventing the formation of full-thickness skin defects. Local administration of deferoxamine (DFO) at wound sites has been shown to promote neovascularization and enhance wound healing. However, since DPU skin wounds are not full-thickness defects and DFO is hydrophilic, enhancing its transdermal delivery is crucial for effective treatment. Photothermal ablation of stratum corneum, generated by copper sulfide nanoparticles (CuS NPs) under near-infrared (NIR) light irradiation, is a promising method to improve transdermal drug delivery. Meanwhile, CuS NPs-induced photothermal therapy offers excellent antibacterial performance. In this study, DFO and CuS NPs were incorporated into a matrix metalloproteinase (MMPs)-sensitive hydrogel. This hydrogel promotes cell adhesion and is degraded by cell-secreted MMPs, a process crucial for the controlled release of encapsulated DFO and CuS NPs. Under NIR irradiation, the stratum corneum is disrupted, facilitating transdermal DFO delivery and simultaneously eliminating infected bacteria. As a result, the essential requirements for DPU treatment, "facilitating transdermal DFO delivery, promoting angiogenesis, and inhibiting bacterial infection", were achieved simultaneously.

Currently, the increasing prevalence of diabetes has emerged as a significant global public health concern [1]. Diabetic pressure ulcers (DPU), also known as diabetic pressure injuries (DPI), are a common complication of this condition. This progression is gradual, starting with an intact skin structure in the early stages, presenting as redness, swelling, heat, pain, or numbness, and the appearance of non-fading erythema from pressure. As the disease progresses, it goes through several stages of partial-thickness skin loss with the exposed dermis, full-thickness skin loss, full-thickness skin, and tissue loss, unstageable pressure injury, and deep tissue pressure injury, which may eventually lead to amputations [2]. Hence, prompt treatment and early intervention are critical in enhancing patient outcomes and averting severe complications.

The normal wound healing process typically undergoes three stages: inflammation, proliferation, and remodeling [3]. Prolonged exposure to high glucose levels can compromise the functionality of neutrophil granulocytes, rendering DPU more susceptible to bacterial infections [4]. The production of advanced glycation end products can also damage endothelial cell function, resulting in reduced neovascularization, which is not conducive to nutrient transport and waste metabolite disposal [5]. These factors contribute to an extended inflammatory phase in the wound, hindering its normal proliferation and remodeling phases, ultimately leading to the formation of chronic wounds [6]. Therefore, effectively inhibiting bacterial growth and promoting neovascularization are crucial for wound healing in diabetic patients. In recent years, exogenous growth factors like basic fibroblast growth factor (bFGF) and vascular endothelial growth factor (VEGF) have been extensively researched to stimulate angiogenesis in chronic wounds [7]. However, the limited application of exogenous growth factors in wound healing is attributed to their rapid elimination and poor stability [8]. In addition, wounds are commonly infected by various bacteria and fungi, and excessive antibiotic use can foster bacterial resistance [9]. Taken together, it is urgent to develop a more efficient method to overcome these drawbacks and simultaneously achieve both needs of "promoting angiogenesis and effectively killing

* Corresponding author.
E-mail address: shenhj@ujs.edu.cn (H. Shen).
[1] These authors contributed equally to this work.

https://doi.org/10.1016/j.cclet.2024.110283
1001-8417/

drug-resistant bacteria" [10,11]. This endeavor holds significant importance in wound repair for diabetes, which involves multifactorial coordination.

Recent studies have highlighted the potential of deferoxamine (DFO) in promoting wound healing [12]. DFO regulates hypoxia-inducible factor-1α (HIF-1α) levels, resulting in increased expression of genes associated with angiogenesis, such as VEGF, thereby accelerating chronic wound healing [13]. However, systemic delivery of DFO is not a viable therapeutic option for diabetic patients due to its short plasma half-life, the need for frequent injections, and potential toxicity. Consequently, local transdermal drug delivery systems present a more effective solution for clinical use. Notably, in the early stages of wounds, DPU is not full-thickness skin loss. DFO, as a hydrophilic drug, has limited ability to penetrate the skin. Therefore, there is an urgent need to develop a new method to address the issues mentioned above and achieve effective transdermal drug delivery. Lu *et al.* introduced a strategy of photothermal ablation of stratum corneum to enhance transdermal drug delivery. The photothermal ablation was generated by copper sulfide nanoparticles (CuS NPs) under near-infrared (NIR) light irradiation [14]. CuS NPs can convert light energy into heat, disrupting the stratum corneum and creating microchannels for improved drug penetration. This photothermal ablation process facilitated drugs penetrating the skin and entering the bloodstream, leading to therapeutic effects. Notably, this photothermal therapy (PTT) can directly target and destroy bacterial structures by creating local high temperatures. This mechanism helped to broadly inhibit bacterial activity and avoid the risk of drug resistance development [15]. Therefore, we proposed an innovative approach incorporating CuS NPs and DFO into a hydrogel dressing. Under NIR irradiation, photothermal ablation was beneficial for the transdermal delivery of DFO, while PTT would kill drug-resistant bacteria.

Hydrogels have been extensively employed as drug carriers and wound dressings in various applications. However, conventional hydrogels exhibit a physical barrier effect due to their network crosslinking structure, which impedes the migration of cells within the hydrogel. Since DFO can accelerate wound healing by activating the migration and proliferation of cells, such as endothelial cells and fibroblasts, it is crucial to find a way to promote cell migration instead of hindering it when utilizing hydrogels. Matrix metalloproteinases (MMPs) represent a group of enzymes widely involved in extracellular matrix (ECM) remodeling and degradation. In diabetic wounds, continuous hyperglycemia can induce inflammation, increase oxidative stress, and stimulate cells to release elevated levels of MMPs [16]. Recent researches have focused on developing hydrogels that are sensitive to MMPs by incorporating polypeptides containing MMP degradation sites into the crosslinking structure [17]. These polypeptide sequences can be cleaved by MMPs, leading to the degradation of the crosslinked network within the hydrogel, beneficial for cell migration in the hydrogel interior and intelligent drug release. Specifically, in this study, DFO and CuS were loaded into MMPs-sensitive hydrogel and combined with photothermal therapy. In our concept, photothermal treatment can disrupt the stratum corneum, leading to the adhesion of exposed endothelial cells or fibroblasts onto the hydrogel substrate and subsequent degradation of its crosslinked network through cell-secreted MMPs, thereby facilitating cellular migration within the hydrogel matrices. Meanwhile, the degradation of the hydrogel accelerates the release of DFO, further facilitating transdermal absorption and subsequently enhancing cell proliferation and migration. These mutually reinforcing processes synergistically promote wound healing. It is worth noting that as the disease progresses, in later stages such as partial-thickness skin loss with exposed dermis and full-thickness skin loss, cells are more likely to adhere to the hydrogel, and the significance of introducing MMPs-sensitive functions into the hydrogel will become more prominent.

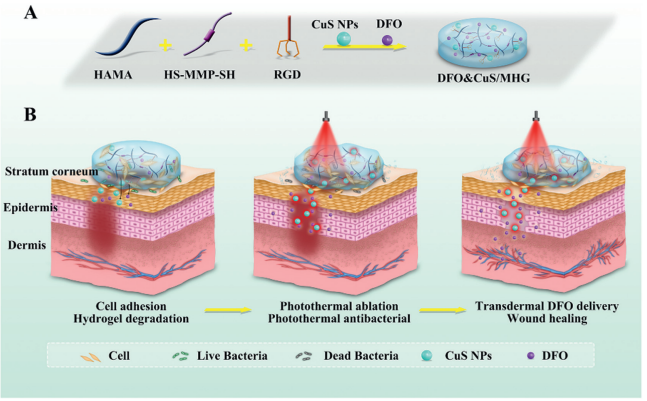

Scheme 1. (A) Schematic diagram of DFO&CuS/MHG preparation process. (B) DFO&CuS/MHG accelerates diabetic pressure ulcer healing by effectively killing drug-resistant bacteria, facilitating transdermal delivery of DFO, and promoting angiogenesis.

In this study, hyaluronic acid (HA) was modified by grafting a cell adhesion peptide (Arg-Gly-Asp, RGD) and subsequently crosslinked with an MMP-degradable peptide (HS-MMP-SH) to engineer an MMP-sensitive HA hydrogel, referred to as MHG. DFO and CuS NPs were encapsulated within this matrix, named DFO&CuS/MHG. According to our proposed concept (Scheme 1), DFO&CuS/MHG is applied to the surface of a pressure ulcer, where the RGD facilitates cell adhesion to the hydrogel. The crosslinked network structure is progressively degraded by MMPs secreted by the adherent cells, enabling the controlled release of encapsulated DFO and CuS NPs. Under NIR light irradiation, the skin stratum corneum is disrupted, and the transdermal delivery of DFO is facilitated. Meanwhile, the infected bacteria at the wound site are eradicated. In conclusion, DFO&CuS/MHG meets all requirements for "effectively killing drug-resistant bacteria, facilitating transdermal DFO delivery, and promoting angiogenesis", thus accelerating the healing of DPU wounds.

Firstly, methacrylated hyaluronic acid (HAMA) was synthesized according to previously reported methods and validated by ^{1}H NMR spectroscopy. As depicted in Fig. S1 (Supporting information), two distinct signal peaks were observed at 5.65 and 6.11 ppm, corresponding to the vinyl proton peaks in acrylate esters. Additionally, a signal peak at 1.84 ppm was identified as the methyl proton peak of acrylate esters. The degree of substitution of the acrylate group was calculated to be 74%, thus confirming the successful synthesis of HAMA. MHG was synthesized through a Michael addition reaction between the acrylate groups on HAMA and the sulfhydryl groups on the MMPs-sensitive peptide. The liquid hydrogel precursor was mixed with HS-MMP-HS and incubated at 37 °C for 30 min, resulting in the formation of a semi-solid, transparent gel (Fig. 1A). Further characterization using scanning electron microscopy (SEM) revealed that MHG had a porous network structure (Fig. 1B). Rheological assessments were subsequently conducted to evaluate the mechanical characteristics of MHG. The results demonstrated that within the frequency range of 10^{-1}–10^{1} Hz, the hydrogel consistently exhibited a higher elastic modulus (G') compared to the viscous modulus (G''), indicating successful formation and excellent structural stability of the hydrogel (Fig. 1C). Furthermore, the influence of temperature on the viscoelastic properties of the hydrogel was investigated. The results demonstrate that the hydrogel's storage modulus (G') and loss modulus (G'') remained unaffected by increasing temperatures. It indicates that the physical network within the hydrogel remains stable even under elevated temperatures and shear forces. These results suggest that the temperature increase induced by PTT does not compromise the stability of the hydrogel (Fig. S2 in Supporting information). Fig. 1D illustrates the swelling curve of hydro-

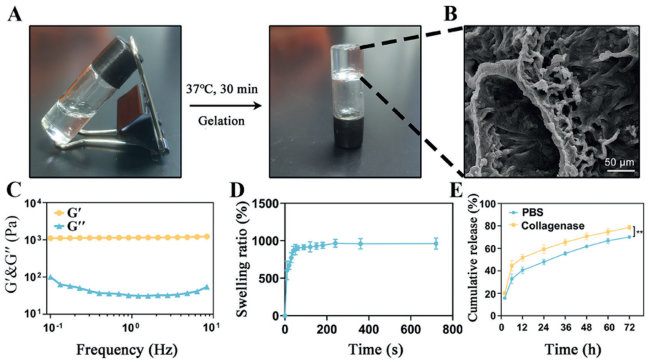

Fig. 1. Fabrication and characterization of MHG. (A) Optical images of the formation of MHG. (B) The SEM picture of MHG. Scale bar: 50 μm. (C) Dynamic frequency scanning test of MHG. (D) Swelling ratio curve of MHG. (E) Cumulative release curve of DFO from MHG in PBS (with or without 1 U/mL collagenase). $^{**}P < 0.01$. Data are expressed as mean ± standard deviation (SD), $n = 3$.

gel, which rapidly achieved an equilibrated swollen state within a few minutes, reaching approximately 966%. To assess the sensitivity of MHG to MMPs, we investigated the release of DFO in different mediums. As depicted in Fig. 1E, the release of DFO in phosphate buffered saline (PBS) buffer containing collagenase was significantly faster than that in standard PBS buffer. This accelerated release was attributed to the degradation of the HS-MMP-SH in MHG by collagenase, facilitating the rapid release of DFO from the hydrogel.

To assess the performance of MHG in promoting cell adhesion, we observed cell morphology through cytoskeleton staining. As shown in Fig. S3 (Supporting information), on day 1, cells exhibited a round and spherical morphology, with fewer cells adhering in the RGD (-) group compared to the RGD (+) group. By day 3, cells in the RGD (+) group appeared more extended and flattened, while cells in the RGD (-) group remained spherical with almost no filamentous protrusions. These findings suggested that the RGD peptide effectively promoted cell adhesion and laid the groundwork for the subsequent *in situ* degradation of the hydrogel. Subsequently, we employed three-dimensional (3D) confocal imaging to investigate cell infiltration in the hydrogel, thereby validating the degradation of the hydrogel. The results in Fig. S4 (Supporting information) revealed that most cells stayed on the surface of the hydrogel crosslinked with dithiothreitol (MMPs-insensitive hydrogel), whereas numerous cells penetrated the interior of the hydrogel crosslinked with HS-MMP-SH (MMPs-sensitive hydrogel). The degradation of the hydrogel network by MMPs may explain the observed phenomenon. With a serum concentration gradient between the upper and lower chambers, cells extended pseudopods and migrated downward in the hydrogel. In conclusion, the above experiments demonstrated that MHG hydrogel promotes cell adhesion and is degraded by cells *in situ*, facilitating drug release.

Subsequently, DFO&CuS/MHG was synthesized, and the photothermal conversion ability of DFO&CuS/MHG was investigated under various power densities. The temperature of DFO&CuS/MHG (containing 200 μg/mL CuS NPs) reached 44.3 °C in 5 min under NIR laser (808 nm, 1.5 W/cm^2) irradiation (Fig. 2A). As the laser power density escalated, the temperature rose to 59.2 °C (2.0 W/cm^2) and 75.4 °C (2.5 W/cm^2) after 5 min of NIR irradiation. Then, hydrogels containing diverse concentrations of CuS NPs were prepared and applied in this experiment to verify the correlation between photothermal performance and CuS NPs concentration (Fig. 2B). The temperature of the hydrogel containing 400 μg/mL of CuS NPs surged from 21.7 °C to 66.5 °C within 5 min (2.0 W/cm^2), demonstrating remarkable photothermal conversion performance. Nevertheless, the blank hydrogel (without CuS NPs) displayed a weaker photothermal heating capacity (approximately 3 °C) under the same conditions. These findings validate that the photothermal conversion effect of DFO&CuS/MHG can be easily adjusted by altering the concentration of CuS NPs and the intensity of NIR irradiation, which is conducive to the practical utility of the hydrogel. Reports have demonstrated that bacteria can be eradicated at 55 °C without harming healthy tissues [18]. Therefore, we adopted a CuS NPs concentration of 200 μg/mL and a laser power of 2.0 W/cm^2 for subsequent investigations. Moreover, DFO&CuS/MHG exhibited outstanding photothermal stability even after undergoing three cycles of alternating NIR irradiation, with only slight temperature fluctuations between adjacent peaks in each cycle (Fig. S5 in Supporting information). These results indicate that the designed DFO&CuS/MHG possesses exceptional photothermal properties and holds promise as a photothermal platform for transdermal drug delivery and antibacterial therapy.

To evaluate the photothermal pro-transdermal properties of DFO&CuS/MHG, we initially examined the photothermal ablation effect on the skin using hematoxylin and eosin (H&E) staining. Skin coated with MHG remained intact following NIR laser irradiation (5 min, 2.0 W/cm^2). In contrast, skin coated with DFO&CuS/MHG exhibited the removal of the epidermal stratum corneum post-irradiation, with no significant damage observed in tissues outside the irradiation site (Fig. 2C). This outcome indicates that the photothermal effect generated by the hydrogel can effectively disrupt the stratum corneum of the skin, laying the groundwork for subsequent transdermal drug delivery. To visualize the transdermal penetration process, fluorescein isothiocyanate-conjugated bovine serum albumin (FITC-BSA) was utilized to mimic a hydrophilic drug and examined *via* fluorescence microscopy. The distribution of FITC-BSA in the skin is depicted in Fig. 2D. In the BSA/MHG + NIR group, the green fluorescence was predominantly confined to the epidermis, with minimal fluorescence detected in the dermis. Conversely, in the BSA&CuS/MHG + NIR group, the green fluorescence spread throughout the epidermis and penetrated the dermis. These findings suggest that the localized heat generated by CuS nanoparticles under NIR irradiation can disrupt the skin stratum corneum, thus facilitating drug penetration. Subsequently, the transdermal penetration of DFO was evaluated *via* an in *vitro* transdermal assay (Fig. 2E). The results revealed that the cumulative permeation rate of the DFO&CuS/MHG + NIR group reached 33.2% after 24 h, while the permeation rate of the DFO/MHG + NIR group was only 16.4% (Fig. 2F). These outcomes signified that the hydrogel containing CuS nanoparticles enhanced DFO transdermal absorption after NIR light irradiation, attributed to its excellent photothermal ablation effect.

To investigate the photothermal antibacterial efficacy of DFO&CuS/MHG, the common pathogenic bacteria *Escherichia coli* (*E. coli*) and methicillin-resistant *Staphylococcus aureus* (MRSA) were employed as models. The colony forming unit (CFU) plate counting assay was initially performed. Fig. 2G demonstrates the absence of any colony growth on the plates from the DFO&CuS/MHG + NIR group, while the plates from the other groups were filled with bacteria (Fig. S6 in Supporting information). It suggests that NIR laser or CuS NPs alone cannot inhibit bacterial growth, and only a combined approach can exert the antibacterial effect. Further exploration of the antibacterial mechanism of the hydrogels involved examining the structural integrity of bacterial cell membranes utilizing the SYTO9/PI staining protocol. As demonstrated in Fig. 2H, treatment of MRSA and *E. coli* with MHG, MHG + NIR, and DFO&CuS/MHG groups resulted in significant green fluorescence, with only a few bacteria exhibiting red fluorescence. In contrast, bacteria treated with the DFO&CuS/MHG + NIR group displayed intense red fluorescence, indicating that nearly all bacteria were eradicated following this treatment. To directly assess the impact of different treatments on bacterial cell membrane damage, SEM was employed to observe

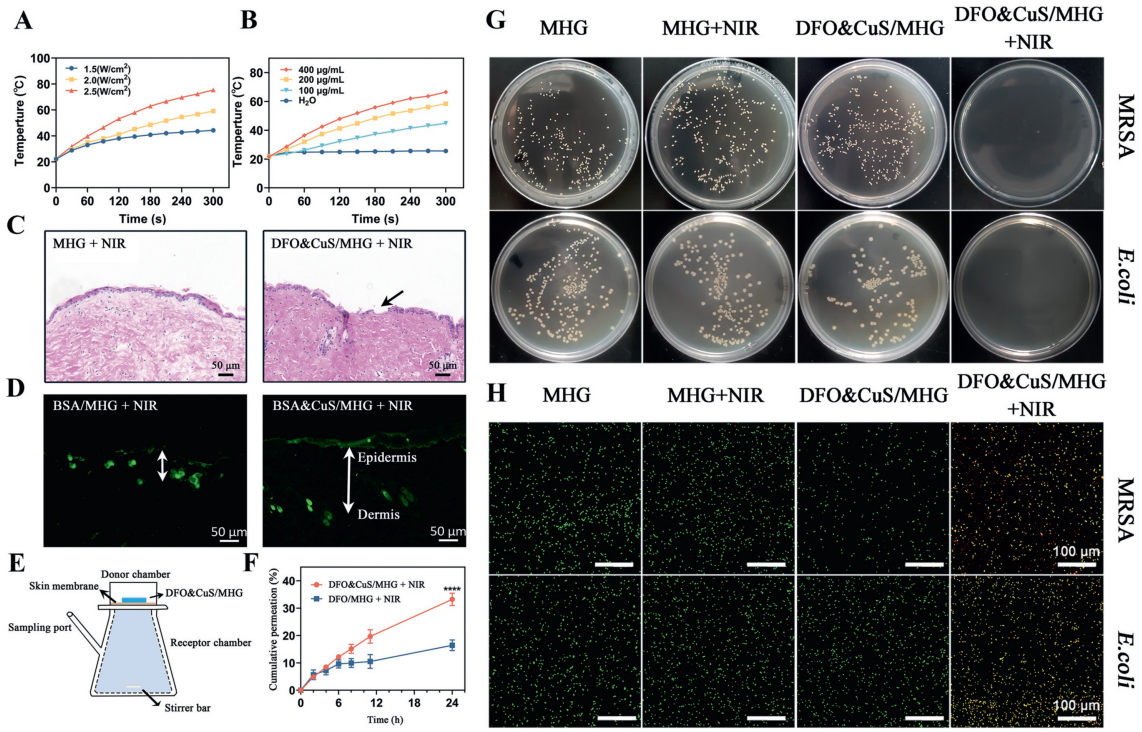

Fig. 2. Characterization of photothermal transdermal and antibacterial properties. (A) Photothermal temperature variation curves under 808 nm NIR irradiation for different laser power densities (1.5, 2.0, and 2.5 W/cm^2). (B) Photothermal temperature variation curves of hydrogels containing different concentrations of CuS NPs (0, 100, 200, and 400 μg/mL) under 808 nm NIR irradiation. (C) H&E images of the skin cross-section treated with MHG + NIR or DFO&CuS/MHG + NIR. Arrows: defects in the epidermal stratum corneum. Scale bar: 50 μm. (D) Fluorescence pictures of the skin cross-section treated with BSA/MHG + NIR and BSA&CuS/MHG + NIR. Scale bar: 50 μm. (E) Schematic illustration of Franz diffusion cell experiment. (F) The cumulative permeation rate of the drug from the DFO/MHG and DFO&CuS/MHG under NIR irradiation. (G) Photographs of MRSA and *E. coli* colonies formed on LB agar plates with different treatments. (H) Representative fluorescence images of MRSA and *E. coli* with different treatments, stained by SYTO9/PI bacterial staining kit. Scale bar: 100 μm. $^{****}P < 0.0001$. Data are expressed as mean ± SD, $n = 3$.

the morphological changes in MRSA and *E. coli* after treatment. As illustrated in Fig. S7 (Supporting information), both MRSA and *E. coli* treated with MHG, MHG + NIR, and DFO&CuS/MHG displayed intact and smooth cell membranes, indicating minimal damage to the bacteria. In contrast, the morphology of MRSA and *E. coli* was disrupted after treatment with DFO&CuS/MHG + NIR, with the cell membranes appearing wrinkled, distorted, and exhibiting holes. These alterations confirmed that the bactericidal effect of DFO&CuS/MHG + NIR primarily occurred by inducing damage to the bacterial cell membranes.

Good cytocompatibility is an essential factor in the application of hydrogel wound dressing. First, we investigated the effect of hydrogel extracts on cell viability using the cell counting kit-8 (CCK-8) assay. Whether NIH-3T3s or human umbilical vein endothelial cells (HUVECs), there was no statistically significant difference between the cell viability of all groups (Figs. S8A and B in Supporting information). The cell viability after 24 h was all higher than 80%. In addition, changes in cell viability after direct contact with the hydrogel were evaluated using live/dead cell staining. The fluorescence images of HUVECs and NIH-3T3s co-cultured with hydrogel after one day are shown in Fig. S9 (Supporting information). Most cells exhibited normal morphology, with minimal detectable red fluorescence, indicating their optimal condition. The above experiments demonstrated that neither indirect incubation with the hydrogel extract nor direct contact with the hydrogel resulted in significant cytotoxicity in the cells. It indicates that DFO&CuS/MHG has good cytocompatibility. Cell migration and angiogenesis play crucial roles in the wound-healing process. Therefore, these aspects were evaluated through cell scratch assay, tubule formation assay, and chicken embryo chorioallantoic membrane (CAM) assay. As revealed by Figs. S10A–D (Supporting information), the scratch area decreased in all groups over time, especially in the DFO&CuS/MHG group. Statistical analysis of the migrated area of NIH-3T3s revealed that the migrated area in the DFO&CuS/MHG group (50.4%) was significantly greater than in the control group (24.4%) and the MHG group (23.6%). The cell scratch assay of HUVECs also showed the same trend, implying that the DFO&CuS/MHG enhances cell migration. In addition, we also conducted a tubule formation experiment to simulate the formation of capillaries *in vitro*. After 6 h of incubation with hydrogel extracts, the HUVECs in the DFO&CuS/MHG group gradually stretched and formed parallel cell lines and branching nodes, and lumen formation was visible. On the other hand, the cells in the other groups only formed some junctions and short lines (Fig. 3A). Quantitative statistical results analyzed by ImageJ were consistent with the microscope observations (Figs. 3C and D). Furthermore, CAM experiments were performed to evaluate the hydrogel proangiogenic ability *in vivo* further. As presented in Fig. 3B, there was a clear difference in blood vessel formation among the control, MHG, and DFO&CuS/MHG + NIR groups. The DFO&CuS/MHG + NIR group exhibited a higher density of vessels with increased capillary counts. Meanwhile, quantitative analysis results indicated that the DFO&CuS/MHG + NIR group induced more extraordinary total vessel lengths than the other groups (Fig. 3E). These experiments demonstrated that DFO&CuS/MHG exhibited favorable proangiogenic properties both *in vitro* and *in vivo*.

Next, we detected the expression of HIF-1α and VEGF by immunofluorescence, Western blot (WB), and quantitative real time polymerase chain reaction (qRT-PCR) experiments. As shown in Fig. 3F and Fig. S11A (Supporting information), after the corresponding treatment, the HIF-1α protein expression in the DFO&CuS/MHG group significantly increased and was localized in the nucleus.

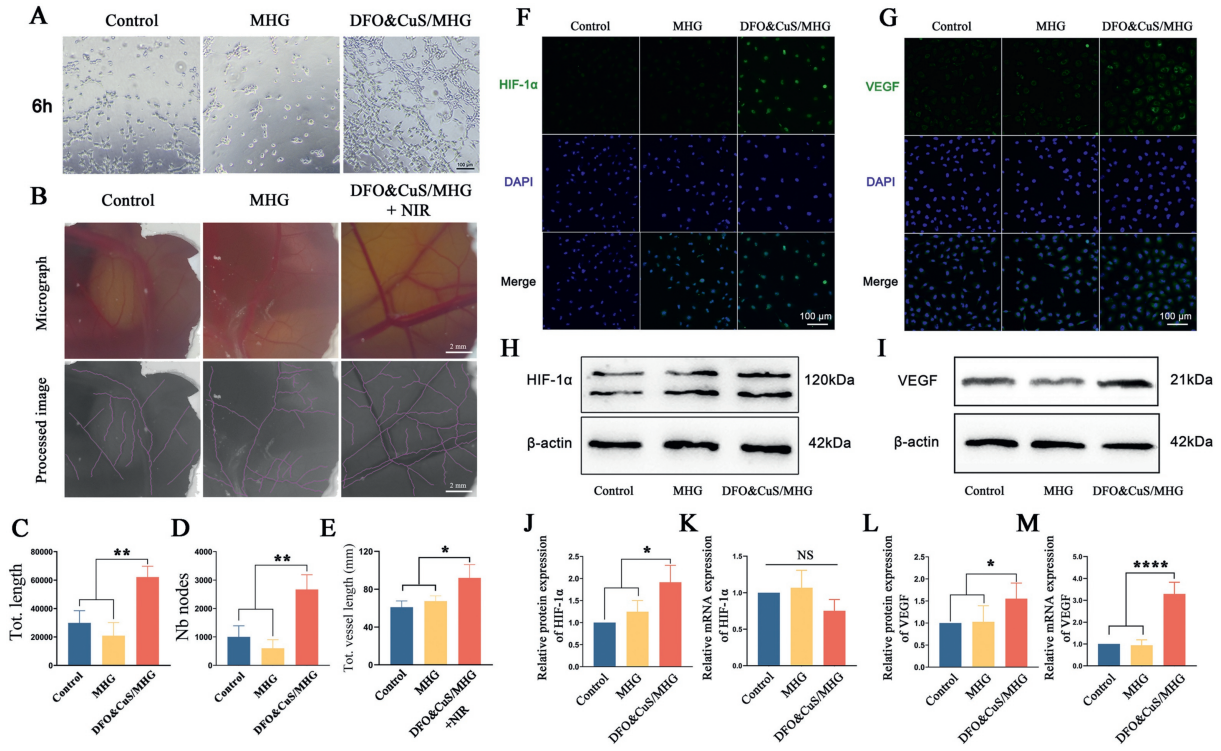

Fig. 3. Pro-angiogenic properties of DFO&CuS/MHG. (A) *In vitro* tubule formation after treatment with different samples for 6 h. Scale bars: 100 μm. (B) Representative images of the blood vessels formed on CAM after different treatments ($n = 3$). Scale bar: 2 mm. Quantification of tubule length (C) and nodes (D). Quantification of total vessel length (E) formed on CAM after different treatments. Immunofluorescence images of different samples stained for HIF-1α (F) and VEGF (G). Scale bar: 100 μm. HIF-1α (H) and VEGF (I) protein expression levels were evaluated by WB analysis. Statistical analysis of HIF-1α protein (J) and mRNA (K) expression level. Statistical analysis of VEGF protein (L) and mRNA (M) expression level. $^{*}P < 0.05$, $^{**}P < 0.01$, $^{****}P < 0.0001$. NS, no significance; DAPI, 4′,6-diamidino-2′-phenylindole. Data are expressed as mean ± SD, $n = 3$.

In contrast, the expression of HIF-1α in the other groups was negligible. As shown in Fig. 3G and Fig. S11B (Supporting information), VEGF protein expression was also increased in the DFO&CuS/MHG group. The results of WB shown in Figs. 3H and I were almost consistent with the findings of immunofluorescence, and the expression of HIF-1α and VEGF in the DFO&CuS/MHG group was 1.91 and 1.55 folds higher than that in the control group, respectively (Figs. 3J and L). Subsequently, we delved into the changes in gene expression levels of these proteins. Interestingly, although VEGF gene expression significantly increased in the DFO&CuS/MHG group, there was no expected elevation in the HIF-1α gene expression; Instead, it displayed a downward trend (Figs. 3K and M). This discrepancy may be attributed to DFO's role in increasing HIF-1α levels by inhibiting its degradation rather than directly regulating the transcriptional activity of the HIF-1α gene. Moreover, the high expression of the downstream protein VEGF might exert a negative feedback effect by suppressing the transcriptional activity of HIF-1α. In conclusion, the results from these experiments successfully demonstrated that DFO&CuS/MHG could promote angiogenesis through the HIF-1α/VEGF axis.

Based on the favorable *in vitro* antibacterial and angiogenic effects, we investigated the efficacy of DFO&CuS/MHG with NIR for treating infected pressure ulcers in diabetic mice (treatment protocol was shown in Fig. S12 in Supporting information). All animal experiments were approved by the Experimental Animal Care and Use Committee of Jiangsu University (UJS-IACUC-2022110901). The wound healing process at days 0, 2, 6, 10, and 14 is depicted in Fig. 4A. Macroscopically, wound healing in the DFO&CuS/MHG + NIR group was faster than in the other groups, and the wound was almost completely healed on day 14. Additionally, the wound images were analyzed using ImageJ software (Fig. 4B). The results showed that the wound area rate in the DFO&CuS/MHG + NIR group on day 6 (63.20%) was notably smaller than that of the control group (89.41%), the MHG group (93.75%), and the DFO&CuS/MHG group (89.61%). This result suggests that the combination of DFO&CuS/MHG with NIR exhibited a significant healing effect in the first week. This is primarily because NIR irradiation can destroy the skin's stratum corneum, promoting the transdermal absorption of DFO. This allows DFO to penetrate the pressure ulcer tissue deeply and exert its efficacy, thereby accelerating the wound healing. In addition, according to the literature, photothermal therapy may have some positive effects on wound healing. It can stimulate local microcirculation and promote cell proliferation and angiogenesis [19]. To further evaluate the wound healing effect of hydrogel, H&E and Masson staining were performed on day 14. After 14 days of treatment, the formation of new granulation tissue was observed in all groups (Fig. 4C). A significant abundance of neutrophils (blue arrows) was noted in control, MHG, and DFO&CuS/MHG groups, indicating persistent inflammation. In contrast, fewer inflammatory cells were found in the DFO&CuS/MHG + NIR group, likely due to the superior photothermal antibacterial properties of DFO&CuS/MHG (Fig. 4D). Collagen deposition is crucial for restoring tensile strength and aiding scar contraction during the remodeling phase [20]. Masson staining was employed to evaluate collagen deposition and remodeling. After 14 days of treatment, the collagen in the wound skin was thicker, denser, and more aligned in the DFO&CuS/MHG + NIR group (Fig. 4E). The collagen content in the DFO&CuS/MHG + NIR group (26.69%) was dramatically higher compared to the control (9.52%), MHG (10.52%), and DFO&CuS/MHG (10.13%) groups, demonstrating excellent tissue regeneration properties (Fig. 4F).

In addition to collagen deposition, angiogenesis is crucial for wound healing. To examine the angiogenesis effect of hydrogels *in vivo*, immunohistochemical (IHC) staining of HIF-1α, VEGF, and CD31 was performed. As shown in Fig. S13A (Supporting information), the staining of HIF-1α and VEGF was the deepest in

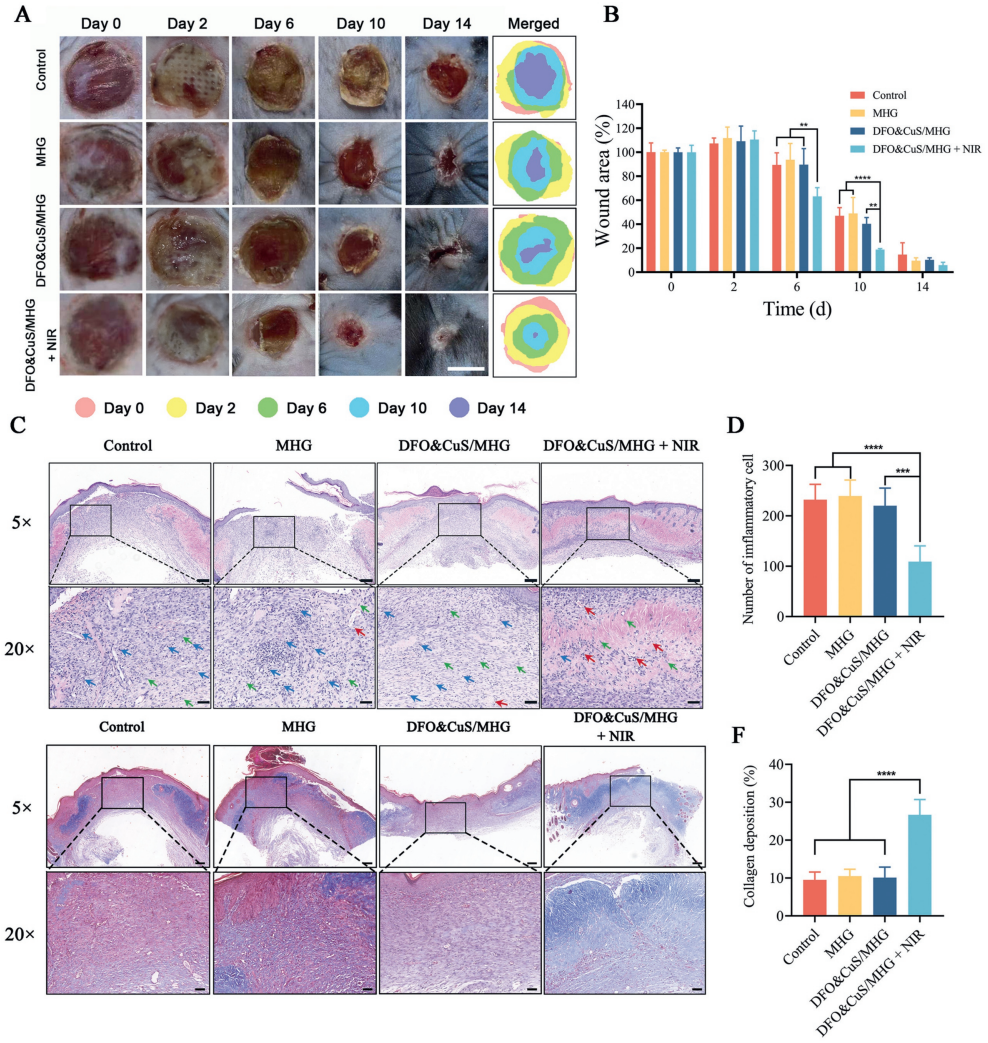

Fig. 4. DFO&CuS/MHG promoted MRSA-infected diabetic pressure wound healing *in vivo*. (A) Representative images of the diabetic wounds treated with different samples from day 0 to day 14. Scale bar: 5 mm. (B) Statistical analysis of the wound area in different treatment groups. (C) H&E staining of wound tissues on day 14 after different treatments. Blue arrow: inflammatory cells; Green arrow: fibroblast cells; Red arrow: blood vessels. Scale bars: 200 μm (5×), 50 μm (20×). (D) Quantitative analysis of the number of inflammatory cells. (E) Masson staining of wound tissues on day 14 after different treatments. Scale bars: 200 μm (5×), 50 μm (20×). (F) Statistical analysis of collagen deposition. $^{**}P < 0.01$, $^{***}P < 0.001$, $^{****}P < 0.0001$. Data are expressed as mean ± SD, $n = 5$.

the DFO&CuS/MHG + NIR group. Statistical results showed that the expression of HIF-1α and VEGF was significantly higher than the other three groups (Figs. S13B and C in Supporting information). IHC staining of CD31 was used to assess neovascularization in the skin wounds. The results indicated that the number of newly formed vessels was the highest in the DFO&CuS/MHG + NIR group, demonstrating the efficacy of the treatment in promoting vascular regeneration at the wound site *in vivo* (Fig. S13D in Supporting information). It is worth noting that despite the multiple benefits of photothermal ablation, there are some risks involved in its utilization, such as thermal damage and excessive tissue ablation. Therefore, precise control of energy and treatment duration is needed in clinical applications to avoid these side effects. Histological analysis of the wound site revealed that following treatment with DFO&CuS/MHG combined with NIR irradiation, the stratum corneum was removed or exfoliated. Importantly, this damage was confined to the stratum corneum and did not harm the viable epidermis. These findings are consistent with previous reports [14], indicating that photothermal therapy does not cause irreversible damage to surrounding healthy tissues. Moreover, due to potential concerns regarding the toxicity of CuS nanoparticles, histological analyses of the major organs (heart, liver, spleen, lungs, and kidneys) were performed on the 14th day after treatment. The results indicated no significant organ damage (Fig. S14 in Supporting information), revealing that DFO&CuS/MHG has good biocompatibility and can be safely applied for wound treatments.

In summary, a matrix metalloproteinase-sensitive hydrogel has been developed as a wound dressing for diabetic patients, effectively encapsulating DFO and CuS NPs to enhance angiogenesis and provide antibacterial properties synergistically. This hydrogel promotes cell adhesion and undergoes degradation by cell-secreted MMPs, facilitating DFO release. When combined with NIR laser, DFO&CuS/MHG disrupts the skin stratum corneum, facilitates transdermal delivery of DFO, and effectively inhibits various bacteria at the wound site. Cell scratch, tubule formation, and CAM experiments have successfully demonstrated that DFO&CuS/MHG can promote angiogenesis. Immunofluorescence, WB, and qRT-PCR assays confirmed upregulated HIF-1α and VEGF expression in HUVECs, thereby supporting DFO's role in activating angiogenesis. Overall, this approach facilitates transdermal DFO delivery, promotes angiogenesis, and inhibits bacterial infection, collectively promoting the healing of infected diabetic pressure ulcers. DFO&CuS/MHG addresses the limitations of existing treatments, offers prolonged action of growth factors, improves efficacy against

drug-resistant bacteria, and enhances transdermal absorption of drugs. This innovation can delay wound deterioration, improve prognosis, and provide a promising treatment option for diabetic pressure ulcers.

Declaration of competing interest

The authors declare that they have no known competing financial interests or personal relationships that could have appeared to influence the work reported in this paper.

CRediT authorship contribution statement

Haijun Shen: Writing – review & editing, Supervision, Project administration, Funding acquisition. **Yi Qiao:** Writing – original draft, Methodology, Investigation, Data curation. **Chun Zhang:** Software, Formal analysis. **Yane Ma:** Methodology, Investigation. **Jialing Chen:** Investigation, Data curation. **Yingying Cao:** Validation, Investigation. **Wenna Zheng:** Validation, Methodology.

Acknowledgments

This work was supported by the National Natural Science Foundation of China (No. 82072044) and the Qing Lan Project of Jiangsu Province of China.

Supplementary materials

Supplementary material associated with this article can be found, in the online version, at doi:10.1016/j.cclet.2024.110283.

References

[1] N.H. Cho, J.E. Shaw, S. Karuranga, et al., Diabetes Res. Clin. Pract. 138 (2018) 271–281.
[2] L.E. Edsberg, J.M. Black, M. Goldberg, et al., J. Wound. Ostomy. Cont. 43 (2016) 585–597.
[3] M.S. Hu, Z.N. Maan, J.C. Wu, et al., Ann. Biomed. Eng. 42 (2014) 1494–1507.
[4] J.M. Ramirez-Acuna, S.A. Cardenas-Cadena, P.A. Marquez-Salas, et al., Antibiotics 8 (2019) 193.
[5] H.N. Wilkinson, M.J. Hardman, Open Biol. 10 (2020) 200223.
[6] V. Falanga, R.R. Isseroff, A.M. Soulika, et al., Nat. Rev. Dis. Primers 8 (2022) 50.
[7] Y.M. Niu, Q. Li, Y. Ding, et al., Adv. Drug Deliv. Rev. 146 (2019) 190–208.
[8] Z.Y. Qian, H.P. Wang, Y.T. Bai, et al., ACS Appl. Mater. Interfaces 12 (2020) 55659–55674.
[9] Z.N. Yi, X.N. Xu, X.H. Meng, et al., Chin. Chem. Lett. 34 (2023) 108238.
[10] R. Zhang, G.H. Jiang, Q.Q. Gao, et al., Nanoscale 13 (2021) 15937–15951.
[11] M. Wang, C.G. Wang, M. Chen, et al., ACS Nano 13 (2019) 10279–10293.
[12] L.Z. Kong, Z. Wu, H.K. Zhao, et al., ACS Appl. Mater. Interfaces 10 (2018) 30103–30114.
[13] J.Z. Zhu, C. Chen, J. Dong, et al., Chin. Chem. Lett. 34 (2023) 107514.
[14] S. Ramadan, L.R. Guo, Y.J. Li, et al., Small 8 (2012) 3143–3150.
[15] Z.K. Hu, H.J. Zhang, Z.Q. Li, et al., Chin. Chem. Lett. 35 (2024) 109527.
[16] D. Kupczyk, R. Bilski, R. Studziñska, et al., Postepy. Dermatol. Alergol. 39 (2022) 59–65.
[17] W. Chen, C.Y. Wang, W. Liu, et al., Adv. Mater. 35 (2023) e2209041.
[18] S.L. Zhu, B.J. Zhao, M.C. Li, et al., Bioact. Mater. 26 (2023) 306–320.
[19] B.D. Zheng, M.T. Xiao, Carbohydr. Polym. 299 (2023) 120228.
[20] S. Sharma, V.K. Rai, R.K. Narang, et al., Life Sci. 290 (2022) 120096.